Evaluation of swelling pressure of bentonite/claystone mixtures from pore size distribution

Zhixiong Zeng, Yu-Jun Cui, Jean Talandier

Evaluation of swelling pressure of bentonite/claystone mixtures from pore size distribution

Zhixiong Zeng[1*], Yu-Jun Cui[1], Jean Talandier[2]

1: Laboratoire Navier/CERMES, Ecole des Ponts ParisTech, 6 et 8 avenue Blaise Pascal, 77455 Marne La Vallée cedex 2, France
2: Andra, 1/7, rue Jean Monnet, 92298 Châtenay-Malabry cedex, France

***Corresponding author**

Zhixiong Zeng

Ecole des Ponts ParisTech
6–8 av. Blaise Pascal, Cité Descartes, Champs-sur-Marne
77455 Marne–la–Vallée cedex 2
France
Tel.: +33 781926608
Fax: +33 164153562
E-mail address: zhixiong.zeng@enpc.fr

Abstract: The swelling behaviour of expansive clays is strongly related to the interaction between clay particles. In this paper, a series of constant-volume swelling pressure and mercury intrusion porosimetry (MIP) tests were carried out on MX80 bentonite/Callovo-Oxfordian (COx) claystone mixtures with different bentonite fractions and dry densities. Results show that the swelling pressure increased linearly with the increase of dry density. Additionally, at a given dry density, the larger the bentonite fraction, the larger the swelling pressure. From the MIP results, the inter-particle pore volume decreased with the increases of bentonite fraction and dry density. To link the macroscopic swelling behaviour with the microstructure features, a new method was proposed, allowing the determination of the average inter-particle distance from the pore size distribution. Moreover, a linear relationship was identified between the swelling pressure and the average inter-particle distance in a semi-logarithmic plane, regardless of the bentonite fraction and montmorillonite content.

Keywords: bentonite/claystone mixture; bentonite fraction; swelling pressure; pore size distribution; inter-particle distance

1 Introduction

Expansive clays are composed of large amount of clay minerals, in particular smectite. Upon contact with water, they develop significant swell or swelling pressure. This swelling behaviour of expansive clays can cause severe distress to civil infrastructures, such as building and roads [5, 15-17, 31, 33]. In some applications, such clays can be greatly beneficial in the case of geological radioactive waste disposal where expansive clays (e.g. bentonite-based materials) are commonly used as sealing material. They are expected to fill up the technological voids and excavation fractures and to generate desired swelling pressure to limit the convergence of the excavation damaged zone [14, 20].

Over the past decades, the swelling behaviour of expansive clays has been extensively studied. It has been well admitted that the swelling behaviour of expansive clays could be influenced by many factors, including mineralogical composition, index properties, dry density, water content, suction, salinity of pore water, etc. [3, 4, 10, 26, 27, 30]. This allowed many empirical and semi-empirical relationships to be proposed according to the relationships between the swelling pressure/swell and influencing factors. Zeng et al. [34, 38, 39] clarify the contribution of claystone to the global swelling pressure of bentonite/claystone mixtures by considering the interaction between bentonite and claystone in the development of swelling pressure. Xu et al. [28, 29] incorporated the osmotic suction into effective stress for compacted bentonites hydrated with saline solutions, and then developed the correlation between montmorillonite void ratio and effective stress using a fractal model. The fundamental swelling mechanism of expansive clays were also investigated at microscopic scales. Saiyouri et al. [19] suggested that the swelling of clay minerals comprised two main processes: crystalline and osmotic swelling. The crystalline swelling was a process whereby 0-4 discrete layers

of water molecules were placed along the clay monolayers inside particles with a subdivision of the particles into thinner ones that are composed of less stacked clay layers [2, 9, 19]. The cations are attracted to the negatively charged clay particles due to the isomorphous substitution in the crystal lattice (Fig. 1) and the concentration of adsorbed cations near the surface of clay particles is much higher than that far from the surface [24]. This allows the diffuse double layers to be developed on a parallel assembly of clay particles. In that case, the osmotic swelling represented by the interaction of clay particles become dominant. It includes the attractive (van der Waals) and repulsive (diffuse double layer) forces between the clay particles, both of which are highly dependent on the inter-particle distance. To further clarify the swelling behaviour, the inter-particle distance was commonly estimated from the total clay void ratio (or the inter-particle water volume) and the specific surface area [8, 19, 21]. However, the used specific surface area was in general a total value, which included the interlayer zones apart from the inter-particle zones [12]. Moreover, it was assumed that the specific surface could decrease owing to the reduction of unit layer number inside the clay particles during the crystalline swelling process [19, 21]. To address these issues, Liu [9] introduced an empirical parameter related to the average number of the unit layers per clay particle and empirically determined the inter-particle distance from the total void ratio, the thickness of unit layers and the distance between the unit layers. Although reasonable prediction results have been obtained on some specific expansive clays, the applicability of relevant theories to other types of expansive clays is quite limited.

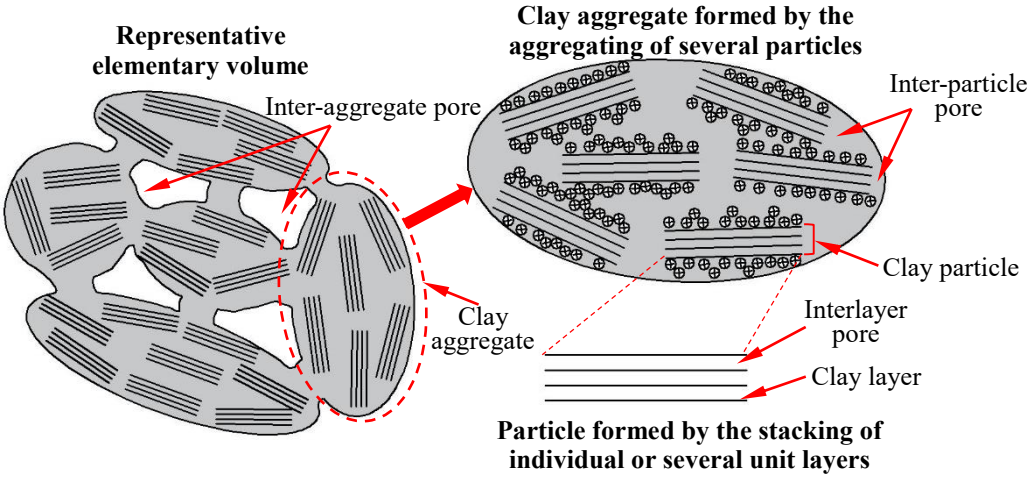

Fig. 1 Fabric units and pore spaces of compacted clay (modified after Liu [9] and Mašín and Khalili [12])

To this end, this study experimentally determined the inter-particle distance and its relationship with the swelling pressure. Firstly, constant-volume swelling pressure tests were performed on compacted MX80 bentonite/Callovo-Oxfordian (COx) claystone mixtures which has been proposed as possible sealing/backfilling materials in the French deep geological disposal for high-level radioactive waste [34]. The swelling pressures of the mixtures with different bentonite fractions (B) and dry densities (ρ_d) were experimentally determined. After the swelling tests, the pore size distributions were investigated using mercury intrusion porosimetry (MIP) and the inter-particle distance was estimated, enabling interpretation of the swelling pressure at a microscopic scale.

2 Materials and methods

The studied soils were the mixtures of MX80 bentonite and COx claystone. The MX80 bentonite was collected from Wyoming in the USA, while the COx claystone was sampled from the Underground Research Laboratory (URL) at around 490 m depth in Bure, France. The bentonite and claystone were then crushed to particles passing through the 2 mm sieve. The physical properties and mineralogical compositions of the bentonite and claystone are listed in Table 1. To simulate the working environment of the sealing/backfilling materials, synthetic site water, which has the same chemical

composition as the site water in the URL, was used as saturation water in the swelling pressure tests. The details about the preparation of the synthetic water can be found in Zeng et al. [35].

The bentonite and claystone powders at their respective initial water contents were well mixed with different proportions of 0/100, 10/90, 20/80, 30/70, 50/50 and 70/30 in dry mass. The corresponding bentonite fractions of the mixtures are 0, 10, 20, 30, 50 and 70%. The specimens of 50 mm diameter and 10 mm height were prepared by static compaction in a rigid steel ring using an axial press at a controlled rate of 0.05 mm/min. The target dry densities of the specimens are shown in Table 2.

Table 1 Physical properties and mineralogical compositions of MX80 bentonite and COx claystone

Soil property	MX80 bentonite	COx claystone
Water content (%)	11.4	6.1
Specific gravity	2.76	2.70
Liquid limit (%)	494	41
Plastic limit (%)	46	24
Plasticity index (%)	448	17
Main minerals	Smectite (86%)	Interstratified illite-smectite (40-45%)[a]
	Quartz (7%)	Carbonate (30%)[a]
	Carbonate and feldspar (7%)	Quartz and feldspar (25-30%)[a]

[a] After Fouché et al. [6]

After compaction, the specimens were transferred to the testing cell (50 mm in inner diameter), as shown in Fig. 2. The compacted specimens were placed between two metallic porous disks and filter papers. These metallic porous disks were specially designed to minimize the deformation of the apparatus. On the top, a piston blocked with a screw was used to restrain the axial deformation during the hydration and a force transducer was installed under the cell to monitor the axial swelling force. The specimens were hydrated by synthetic water from the bottom of the cell at a water head of about 1.0 m and the swelling force during the hydration was recorded by a data logger. All tests were

performed in a temperature controlled room (20±1 °C).

Table 2 Test program and main results

Test No.	Bentonite fraction B (%)	Dry density of specimen ρ_{dm} (Mg/m^3)	Initial water content w_m (%)	Final swelling pressure P_s (MPa)
S01	70	1.38	9.8	0.43
S02	70	1.50	9.8	1.11
S03	70	1.63	9.8	2.53
S04	70	1.71	9.8	3.94
S05	50	1.27	8.8	0.13
S06	50	1.56	8.8	0.85
S07	50	1.73	8.8	2.10
S08	50	1.76	8.8	2.91
S09	30	1.50	7.7	0.22
S10	30	1.60	7.7	0.46
S11	30	1.68	7.7	0.78
S12	30	1.79	7.7	1.59
S13	30	1.89	7.7	2.72
S14	30	1.99	7.7	5.23
S15	20	1.60	7.2	0.26
S16	20	1.69	7.2	0.44
S17	20	1.77	7.2	0.70
S18	20	1.88	7.2	1.93
S19	10	1.61	6.6	0.14
S20	10	1.68	6.6	0.23
S21	10	1.78	6.6	0.39
S22	10	1.90	6.6	1.07
S23	0	1.80	6.1	0.15
S24	0	1.90	6.1	0.47
S25	0	1.99	6.1	0.79

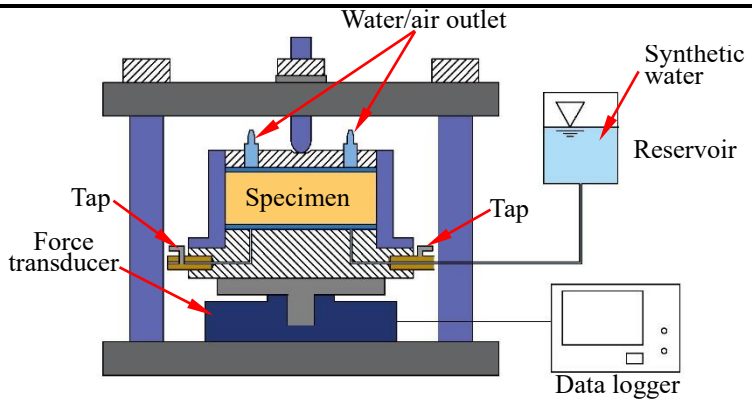

Fig. 2 Layout of the experimental setup for swelling pressure tests

After the swelling pressures tests, the specimens were extracted from the cell and rapidly cut into several cubes (maximum volume of 1 cm^3). The entire operations (removal and cutting) were completed in less than 5 min to minimise the influences of stress release and water evaporation. Prior to the MIP tests, the specimens were freeze-dried following the procedure proposed by Delage and Lefebvre [1] to minimise the microstructure disturbance during dehydration. Autopore IV 9500 mercury intrusion porosimeter was used to explore the pore structure of specimens. The exploration was performed in two stages: a low-pressure phase with a working pressure from 3.6 to 200 kPa; a high-pressure phase with a working pressure from 0.2 to 228 MPa. Note that the influence of mercury pressure on the pore structure was believed to be limited. The pore entrance diameter D (μm) at a mercury pressure p (MPa) could be calculated according to the Washburn equation:

$$D=\frac{4T_s\cos\alpha}{p} \tag{1}$$

where T_s is the interfacial tension (taken as 0.485 N/m); α is the contact angle between the mercury-air interface and soil (taken as 130°). According to Eq. (1), the applied working pressures correspond to a maximum entrance pore diameter of 350 μm and a minimum entrance diameter of 5.5 nm.

3 Experimental results and discussions

3.1 Swelling pressure

When water infiltrated into the specimens, the swelling pressure increased and then tended to stabilization after 2.5-102 h [34]. The variations of stabilized swelling pressure with dry density for the specimens with different bentonite fractions are shown in Table 2 and Fig. 3. For comparison, also presented in the same figure are the results collected from other studies on pure MX80 bentonite [7] and on pure COx claystone [23]. It clearly shows that the swelling pressure increased with the

increase of dry density. There was a linear relationship between the logarithm of swelling pressure and dry density for the specimens with various bentonite fractions. Additionally, the slopes of the fitted lines were almost the same while the intercept of the fitted lines increased with the increasing bentonite fraction. This suggests that the increase of the bentonite fraction enhanced the swelling capacity of the mixtures.

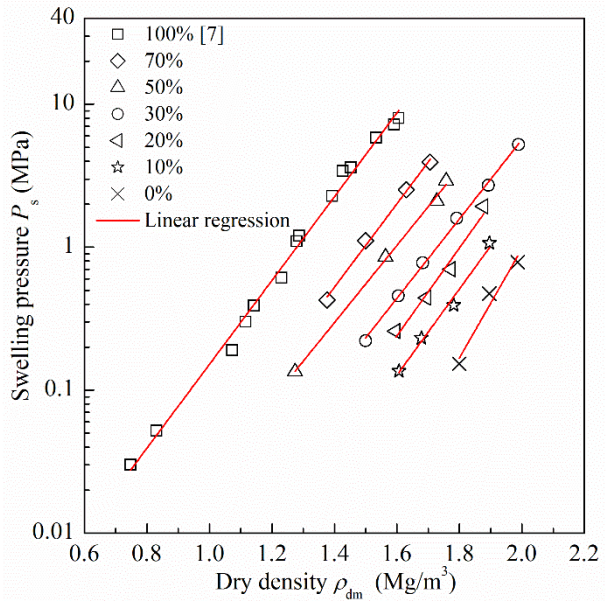

Fig. 3 Variation of the stabilized swelling pressure with specimen dry density

3.2 Pore size distribution

Figs. 4 and 5 presents the typical pore size distribution of the as-compacted specimens with 30% bentonite and those of specimens with different dry densities and bentonite fractions after hydration, respectively. The curves are illustrated in terms of cumulative and density functions in a semi-logarithmic plot. The cumulative curves were well ordered with respect to the dry density: the curve for a lower dry density lied above the curve for a higher dry density. From the density curves, a typical bimodal porosity was observed on the specimens in the as-compacted state, with intra-aggregate pores (inter-particle pores) and inter-aggregate pores [36] (Fig. 4). By contrast, a trimodal porosity was

identified for specimens after swelling, especially for those with low dry densities and low bentonite fractions (Fig. 5). The three main pore populations were at a mean pore diameter of 10-22 μm for large pores, 0.17-0.52 μm for medium pores and around 0.025 μm for small pores. When the as-compacted specimen was hydrated with water, water molecules would infiltrate into the interlayer space and intercalate stepwise between the clay sheets, layer after layer up to 4 layers. In this process, the aggregates swelled and progressively invaded the initial inter-aggregate space. Consequently, an increase in inter-particle pore volume and a decrease in the inter-aggregate pore volume were expected, and a new population (medium pores) appeared with the transformation of some initial inter-particle and inter-aggregate pores into medium-pore size. In case of confined conditions, the swelling of clay minerals would be related to the dry density of clay minerals in the specimens. For the specimens with a larger bentonite fraction and dry density, a higher dry density of clay minerals could be expected and the swelling of aggregate was not allowed to be fully developed; for the specimens with a lower bentonite fraction and dry density, a lower dry density of clay minerals would lead to more significant development of inter-particle space. This explained why a lower small-pore peak value and a larger medium-pore volume were observed for the specimens with a lower bentonite fraction and dry density after saturation (Fig. 5).

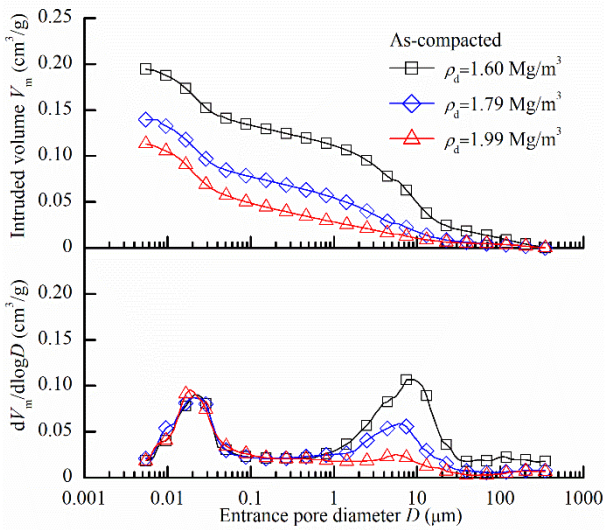

Fig. 4 Pore size distributions of specimens with 30% bentonite.

3.3 Inter-particle distance and its relationship to swelling pressure

As discussed earlier, the inter-particle interactions are directly related to the swelling behaviour. For the bentonite/claystone mixtures, some inter-particle and inter-aggregate pores would merge into medium pores upon hydration, which added a degree of complexity while separating the inter-particle and inter-aggregate pores. Romero et al. [18] and Yuan et al. [32] suggested that the boundary between inter-particle and inter-aggregate pores would be taken at the merged peak when they studied the microstructural behaviour of expansive clays hydrated under free-swell and confined conditions. Following their suggestions, the delimiting diameters between inter-particle and inter-aggregate pores are marked by dash dot lines in Fig. 5. The delimiting diameter ranged from 78.7 to 582.8 nm for the bentonite/claystone mixtures, and the larger the dry density and the bentonite fraction the lower the delimiting value. As the interlayer distance of clay minerals is approximately equal to 2.16 nm with 4 layers of water molecules, the inter-particle distance should be larger than 2.16 nm [19]. Imperfectly, the inter-particle pores with a dimeter ranging from 2.16 to 5.5 nm could not be covered by the used

mercury intrusion porosimetry. In further analysis, the dV/dlog$D$ in the range of 2.16-5.5 nm was estimated using linear extrapolation according to the density function curves. Then, multiplying the dV/dlog$D$ by the pore dimeter yielded the inter-particle pore volume increment in the range of 2.16-5.5 nm. In Fig. 5, the estimated pore size distributions in the range of 2.16-5.5 nm is presented by dash lines. According to the cumulative curves and the delimiting values, the total inter-particle pore volume in 1 g dry soils ($V_{\text{inter-particle}}$ in cm^3/g) for the specimens with different bentonite fractions and dry densities were determined and the obtained results are shown in Fig. 6a. On the whole, the inter-particle pore volume decreased as the dry density and bentonite fraction increased because of the inhibition effect of increasing clay mineral density on the swelling of aggregates. In Fig. 6b, the swelling pressure is plotted versus the inter-particle pore volume. It appears that the swelling pressure increased with the increase of $V_{\text{inter-particle}}$. The relationship between the swelling pressure and $V_{\text{inter-particle}}$ was dependent on the bentonite fraction. At the same $V_{\text{inter-particle}}$, the higher the bentonite fraction, the larger the swelling pressure. Upon the saturation of bentonite/claystone mixtures, clay minerals would form a matrix, the property of which governed the macroscopic swelling behaviour. By contrast, the inert quartz, carbonate or feldspar grains (mainly from the COx claystone) were embedded into the clay matrix [13]. Generally, the small intra-grain pore volume in inert minerals could be ignored [22] and the abovementioned inter-particle pores were resident in the clay matrix. Therefore, to achieve a given swelling pressure, a smaller $V_{\text{inter-particle}}$ was needed for the specimens with larger contents of inert minerals.

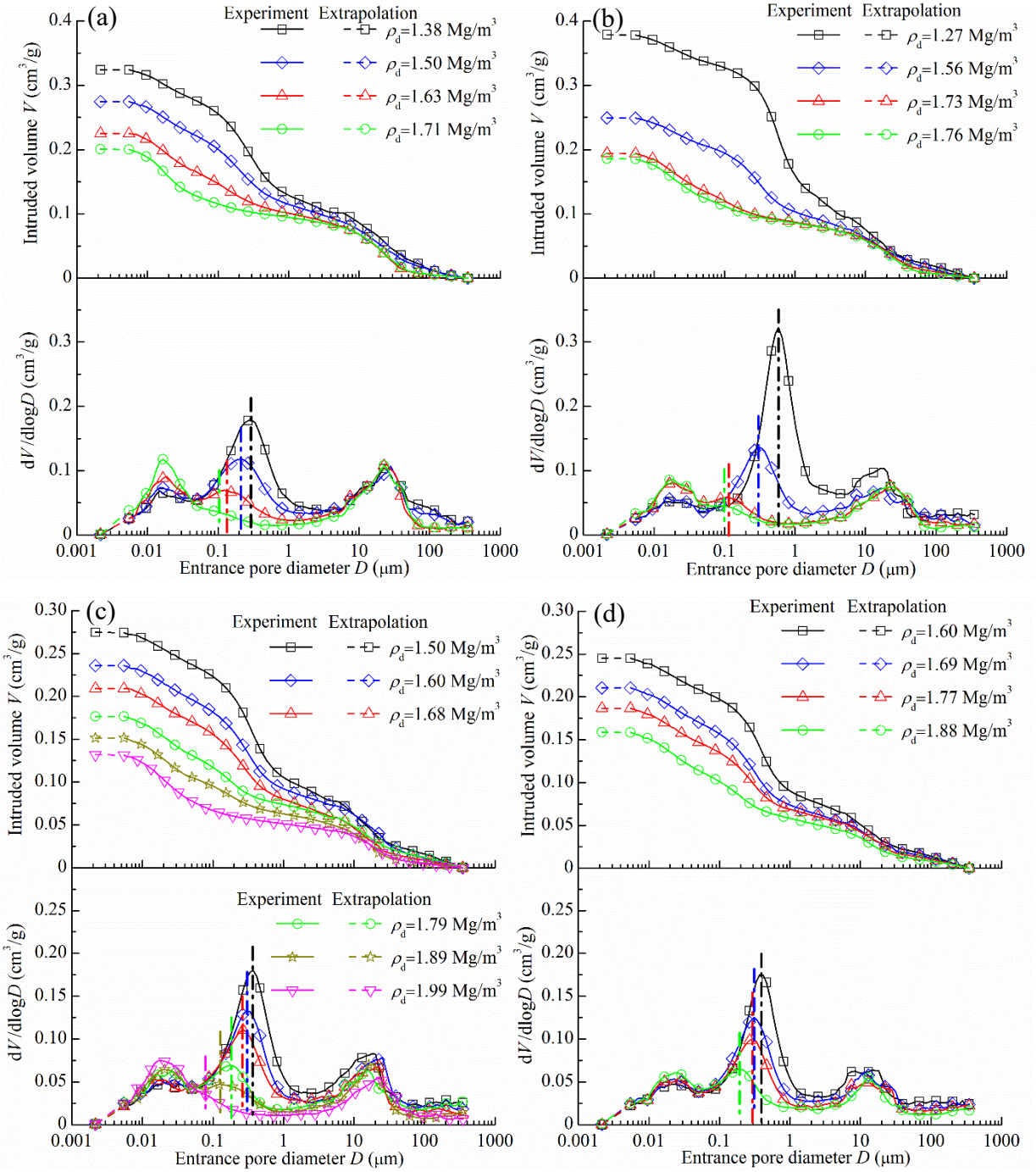
(a)
Experiment Extrapolation
ρ_d=1.38 Mg/m^3
ρ_d=1.50 Mg/m^3
ρ_d=1.63 Mg/m^3
ρ_d=1.71 Mg/m^3
Intruded volume V (cm^3/g)
dV/dlog$D$ (cm^3/g)
Entrance pore diameter D (μm)
(b)
Experiment Extrapolation
ρ_d=1.27 Mg/m^3
ρ_d=1.56 Mg/m^3
ρ_d=1.73 Mg/m^3
ρ_d=1.76 Mg/m^3
Intruded volume V (cm^3/g)
dV/dlog$D$ (cm^3/g)
Entrance pore diameter D (μm)
(c)
Experiment Extrapolation
ρ_d=1.50 Mg/m^3
ρ_d=1.60 Mg/m^3
ρ_d=1.68 Mg/m^3
Experiment Extrapolation
ρ_d=1.79 Mg/m^3
ρ_d=1.89 Mg/m^3
ρ_d=1.99 Mg/m^3
Intruded volume V (cm^3/g)
dV/dlog$D$ (cm^3/g)
Entrance pore diameter D (μm)
(d)
Experiment Extrapolation
ρ_d=1.60 Mg/m^3
ρ_d=1.69 Mg/m^3
ρ_d=1.77 Mg/m^3
ρ_d=1.88 Mg/m^3
Intruded volume V (cm^3/g)
dV/dlog$D$ (cm^3/g)
Entrance pore diameter D (μm)

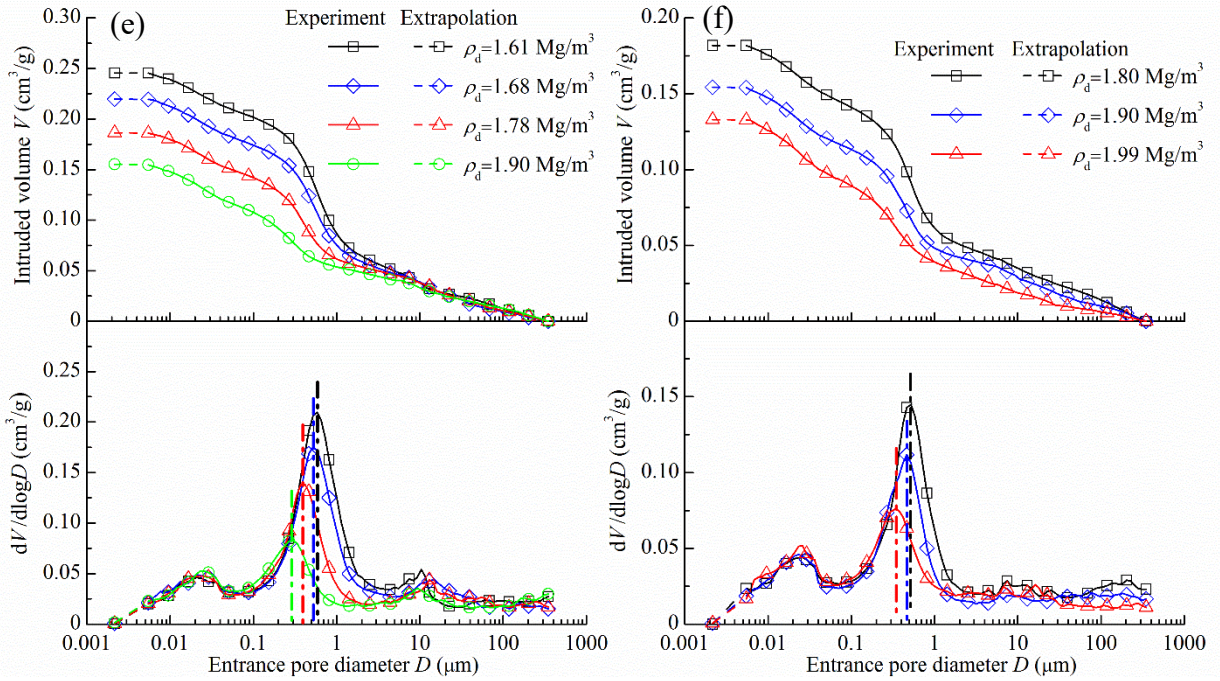

Fig. 5 Pore size distributions of specimens with (a) 70%, (b) 50%, (c) 30%, (d) 20%, (e) 10% and (f) 0% bentonite. Note: the dash dot lines represent the delimiting diameters between inter-particle and inter-aggregate pores

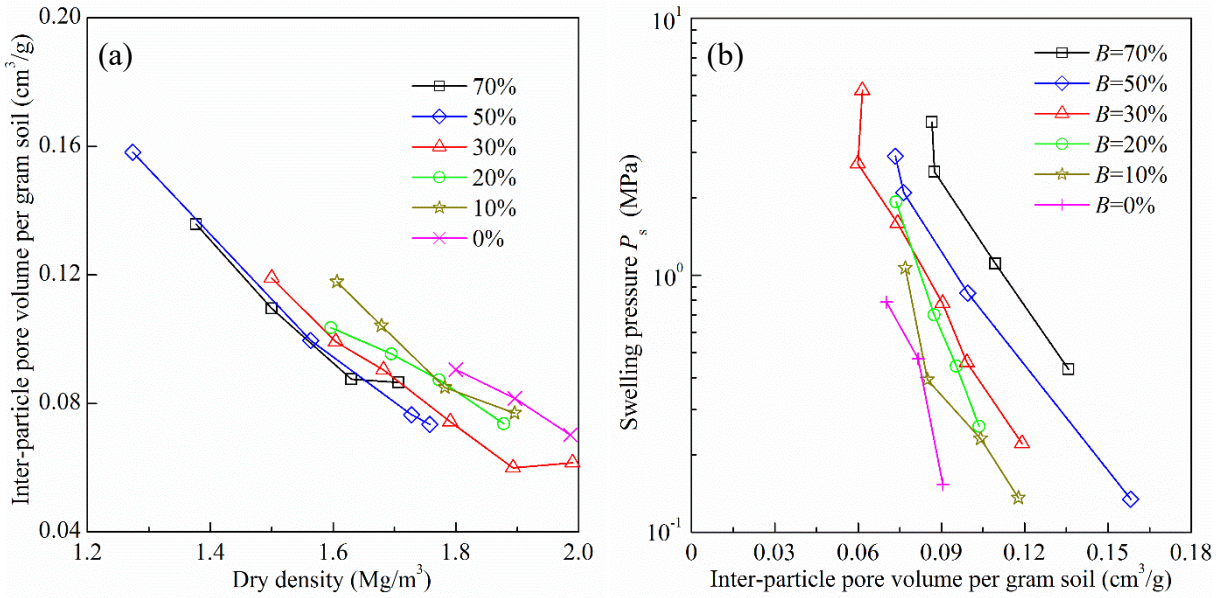

Fig. 6 Variation of the inter-particle pore volume with specimen dry density (a) and variation of the swelling pressure with inter-particle volume (b)

To exclude the influence of inert minerals, the inter-particle distance of clay matrix was determined. For the inter-particle pores with a diameter of D_i (μm) in 1 g dry soil, the total length L_i (μm) could be determined by Eq (2) assuming that the pores were cylindrical [15]:

$$L_i=\frac{10^{12}V_i}{S_i}=\frac{4\times10^{12}V_i}{\pi D_i^2} \quad (2)$$

where S_i (μm^2) is the cross-section area of inter-particle pores with a diameter of D_i and V_i (cm^3) is the volume of inter-particle pores with a diameter of D_i in 1 g dry soils, which could be determined according to the cumulative curves (Fig. 5). Then, the surface area A_i (m^2) was calculated using Eq. (3):

$$A_i=10^{-12}\pi D_i L_i=\frac{4V_i}{D_i} \quad (3)$$

Correspondingly, the total surface area of inter-particle pores $A_{\text{inter-particle}}$ (m^2/g) could be computed:

$$A_{\text{inter-particle}}=\sum_{i=1}^{N}\frac{4V_i}{D_i} \quad (4)$$

where N is the number of pore intervals; i is the counter from 1 to N. According to the inter-particle pore volume and total surface area, the average inter-particle distance $\overline{D}$ (nm) could be estimated by assuming that the clay particles are parallel [11]:

$$\overline{D}=\frac{2\times10^3 V_{\text{inter-particle}}}{A_{\text{inter-particle}}} \quad (5)$$

The average inter-particle distances for the specimens with various bentonite fractions and dry densities are summarized in Fig. 7a. During the hydration, the clay minerals in the bentonite/claystone mixtures, such as smectite, swelled and formed a matrix, while the inert minerals, such as quartz and feldspar, constituted the inclusion and were dispersed in the matrix [37]. Since the quartz and feldspar were generally nonporous, the inter-particle pores existed in the matrix and the obtained inter-particle distance represented the property of the matrix. It appears that the average inter-particle distance decreased with the increase of specimen dry density. For the specimens at the same dry density, the larger the bentonite fraction, the lower the average inter-particle distance. This phenomenon could be

related to the high sensitivity of surface area to the small pores. For the specimens with a larger bentonite fraction, the larger clay mineral density would restrain the swelling of clay particles upon hydration and a larger small-pore volume was expected, compared to those with a lower bentonite fraction. Thereby, a large surface area and a lower average distance were obtained according to Eqs. (3), (4) and (5).

Fig. 7b depicts the relationship between the swelling pressure and the average inter-particle distance. For all specimens, the swelling pressure decreased with the increase of average inter-particle distance, whatever the bentonite fraction. A good correlation can be obtained between the swelling pressure P_s (MPa) and the average inter-particle distance in a semi-logarithmic plot:

$$P_s=29.393\exp^{-0.250\overline{D}} \quad (6)$$

This indicated that the swelling pressure of bentonite/claystone mixtures could be well described by the average inter-particle distance upon hydration. Note however that the bentonite/claystone mixtures reported in this study were hydrated with synthetic water, which had a negligible effect on the swelling behaviour [25]. The influence of chemistry pore solution on relationship between the swelling pressure and inter-particle distance needs to be investigated in-depth in further studies.

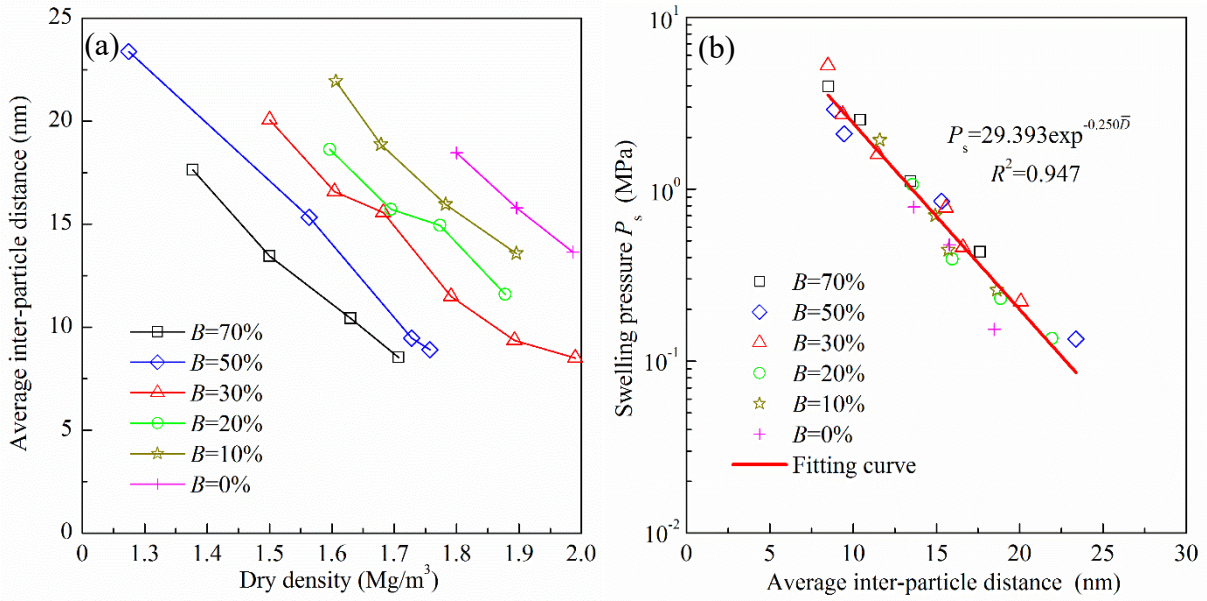

Fig. 7 Variation of the average inter-particle distance with specimen dry density (a) and variation of the swelling pressure with average inter-particle distance (b)

4 Conclusions

In this study, the swelling pressures and microstructure features of MX80 bentonite/COx claystone mixtures with different bentonite fractions and dry densities were experimentally determined, allowing the swelling pressure to be interpreted at a microscopic scale. According to the obtained results, the following conclusions were drawn.

The swelling pressure increased linearly with the specimen dry density. As a given dry density, the swelling pressure increased as the bentonite fraction increased, confirming that the addition of bentonite enhanced the swelling pressure of the mixtures.

The bentonite/claystone mixtures after hydration exhibited a trimodal porosity, with a large pore population with a mean pore diameter of 10-22 μm, a medium pore population with a mean diameter of 0.17-0.52 μm and a small pore population with a mean diameter of 0.025 μm. As the bentonite fraction and dry density increased, the inter-particle pore volume decreased because of the inhibition effect of increasing clay mineral density on the swelling of aggregates.

According to the pore size distribution, the total surface area of inter-particle pores was calculated assuming parallel and cylindrical pores, and the average the inter-particle distance was defined as the ratio of the total volume to the total surface area of inter-particle pores. For the bentonite/claystone mixtures with various bentonite fractions, a linear relationship between the logarithm of swelling pressure and inter-particle distance was identified, showing that the swelling behaviour was mainly dependent on the inter-particle distance after hydration.

Notably, the inter-aggregate pores could also change during the hydration under constant-volume conditions. The global swelling pressure was supported by the structure of aggregates and its stiffness could be related to the pores between aggregates. The relationships between the inter-aggregate pores, aggregate structure stiffness and the global swelling pressure will be investigated in further studies.

Acknowledgments

The supports from the Chinese Scholar Council (CSC) and the French National Radioactive Waste Management Agency (Andra) are greatly acknowledged.

References

1. Delage P, Lefebvre G (1984) Study of the structure of a sensitive Champlain clay and its evolution during consolidation. Can Geotech J 21 (1): 21–35
2. Delage P, Marcial D, Cui YJ, Ruiz X (2006) Ageing effects in a compacted bentonite: a microstructure approach. Géotechnique 56(5): 291-304
3. Du JP, Zhou AN, Lin X, Bu Y, Kodikara J (2020) Revealing expansion mechanism of cement-

stabilized expansive soil with different interlayer cations through molecular dynamics simulations. J Phys Chem C 124(27): 14672-14684

4. Du JP, Zhou AN, Lin X, Bu Y, Kodikara J (2021) Prediction of swelling pressure of expansive soil using an improved molecular dynamics approach combining diffuse double layer theory. Appl Clay Sci 203: 105998

5. Eyo EU, Ng'ambi S, Abbey SJ (2019) Effect of intrinsic microscopic properties and suction on swell characteristics of compacted expansive clays. Transp Geotech 18: 124-131

6. Fouché O, Wright H, Le Cléac'h JM, Pellenard P (2004) Fabric control on strain and rupture of heterogeneous shale samples by using a non-conventional mechanical test. Appl Clay Sci 26(1–4): 367–387

7. Karnland O, Nilsson U, Weber H, Wersin P (2008) Sealing ability of Wyoming bentonite pellets foreseen as buffer material–laboratory results. Phys Chem Earth Parts A/B/C 33: S472-S475

8. Komine H, Ogata N (2004) Predicting swelling characteristics of bentonites. J Geotech Geoenviron Eng 130(8): 818-829

9. Liu L (2013) Prediction of swelling pressures of different types of bentonite in dilute solutions. Colloids Surf A 434: 303-318

10. Ma TT, Yao CQ, Dong Y, Yi PP, Wei CF (2019) Physicochemical approach to evaluating the swelling pressure of expansive soils. Appl Clay Sci 172: 85-95

11. Madsen FT, Müller-Vonmoos M (1985) Swelling pressure calculated from mineralogical properties of a Jurassic opalinum shale, Switzerland. Clays Clay Miner 33(6): 501-509

12. Mašín D, Khalili N (2015) Swelling phenomena and effective stress in compacted expansive clays.

Can Geotech J 53(1): 134-147

13. Menaceur H, Delage P, Tang AM, Talandier J (2016) The status of water in swelling shales: an insight from the water retention properties of the Callovo-Oxfordian claystone. Rock Mech Rock Eng 49(12): 4571-4586

14. Middelhoff M, Cuisinier O, Masrouri F, Talandier J, Conil N (2020) Combined impact of selected material properties and environmental conditions on the swelling pressure of compacted claystone/bentonite mixtures. Appl Clay Sci doi: 10.1016/j.clay.2019.105389.

15. Pedarla A, Puppala AJ, Hoyos LR, Chittoori B (2016) Evaluation of swell behavior of expansive clays from internal specific surface and pore size distribution. J Geotech Geoenviron Eng 142(2): 04015080

16. Puppala AJ, Pedarla A, Hoyos LR, Zapata C, Bheemasetti TV (2016) A semi-empirical swell prediction model formulated from 'clay mineralogy and unsaturated soil' properties. Eng Geol 200: 114-121

17. Puppala AJ, Pedarla A, Pino A, Hoyos LR (2017) Diffused double-layer swell prediction model to better characterize natural expansive clays. J Eng Mech 143(9): 04017069

18. Romero E, DELLA VECCHIA G, Jommi C (2011) An insight into the water retention properties of compacted clayey soils. Géotechnique 61(4): 313-328

19. Saiyouri N, Hicher PY, Tessier D (2000) Microstructural approach and transfer water modelling in highly compacted unsaturated swelling clays. Mech CF Mater 5(1): 41-60

20. Sellin P, Leupin OX (2013) The use of clay as an engineered barrier in radioactive-waste management–a review. Clays Clay Miner 61(6): 477-498

21. Schanz T, Tripathy S (2009) Swelling pressure of a divalent-rich bentonite: Diffuse double-layer theory revisited. Water Resour Res doi: 10.1029/2007WR006495.

22. Souza RFC, Pejon OJ (2020) Pore size distribution and swelling behavior of compacted bentonite/claystone and bentonite/sand mixtures. Eng Geol 275: 105738

23. Tang CS, Tang AM, Cui YJ, Delage P, Schroeder C, De Laure E (2011) Investigating the pressure of compacted crushed-Callovo-Oxfordian claystone. Phys Chem Earth Parts A/B/C 36 (17-18): 1857-1866

24. Tripathy S, Sridharan A, Schanz T (2004) Swelling pressures of compacted bentonites from diffuse double layer theory. Can Geotech J 41(3): 437-450

25. Wang Q, Tang AM, Cui YJ, Delage P, Gatmiri B (2012) Experimental study on the swelling behaviour of bentonite/claystone mixture. Eng Geol 124: 59-66

26. Xiang GS, Xu YF, Xie S, Fang Y (2017) A simple method for testing the fractal dimension of compacted bentonite immersed in salt solution. Surf Rev Lett 24(03): 1750040.

27. Xiang GS, Ye WM, Xu YF, Jalal FE (2020) Swelling deformation of Na-bentonite in solutions containing different cations. Eng Geol 277: 105757.

28. Xu YF, Xiang GS, Jiang H, Chen T, Chu F (2014) Role of osmotic suction in volume change of clays in salt solution. Applied Clay Science, 101, 354-361.

29. Xu YF (2019) Peak shear strength of compacted GMZ bentonites in saline solution. Engineering Geology, 251, 93-99.

30. Yuan SY, Liu XF, Sloan SW, Buzzi, O.P. (2016) Multi-scale characterization of swelling behaviour of compacted Maryland clay. Acta Geotech 11(4): 789-804

31. Yuan SY, Buzzi O, Liu XF, Vaunat J (2019) Swelling behaviour of compacted Maryland clay under different boundary conditions. Géotechnique, 69(6): 514-525

32. Yuan SY, Liu XF, Romero E, Delage P, Buzzi O (2020) Discussion on the separation of macropores and micropores in a compacted expansive clay. Géotechnique Lett doi: 10.1680/jgele.20.00056.

33. Zeng ZX, Kong LW (2019) Effect of wetting–drying–freezing–thawing cycles on the swelling behaviour of the Yanji mudstone. Environ Earth Sci 78(15): 435

34. Zeng ZX, Cui YJ, Zhang F, Conil N, Talandier J (2019) Investigation of swelling pressure of bentonite/claystone mixture in the full range of bentonite fraction. Appl Clay Sci doi: 10.1016/j.clay.2019.105137

35. Zeng ZX, Cui YJ, Zhang F, Conil N, Talandier J (2020). Effect of technological voids on the swelling behaviour of compacted bentonite/claystone mixture. Can Geotech J doi: 10.1139/cgj-2019-0339

36. Zeng ZX, Cui YJ, Conil N, Talandier J (2020). Effects of technological voids and hydration time on the hydro-mechanical behaviour of compacted bentonite/claystone mixture. Géotechnique doi: 10.1680/jgeot.19.P.220

37. Zeng ZX, Cui YJ, Talandier J (2021). Investigating the swelling pressure of highly compacted bentonite/sand mixtures under constant-volume conditions. Acta Geotech doi: 10.1007/s11440-021-01352-0

38. Zeng ZX, Cui YJ, Talandier J. (2022) An insight into grain interaction in bentonite/claystone mixtures. Acta Geotechnica. 12:1-7.

39. Zeng ZX, Cui YJ, Conil N, Talandier J. (2020). Investigating the contribution of claystone to the swelling pressure of its mixture with bentonite. InE3S Web of Conferences, 195, 03043.